



# Soil Sorptive Potential-Based Paradigm for Soil Freezing Curves

Chao Zhang, A.M.ASCE<sup>1</sup>; and Ning Lu, F.ASCE<sup>2</sup>

**Abstract:** The soil freezing curve (SFC) is a fundamental constitutive relationship between liquid water content and temperature under subzero (0°C or 273.15 K) conditions. SFC governs mechanical and hydrologic behavior of soil in freezing and thawing environments. The state-of-the-art SFC paradigms have been established empirically based on the capillary pressure-based Clapeyron equation. Two practical challenges prevent the rigorous use of the capillary pressure-based Clapeyron equation for realistic prediction of the SFC: (1) unable to use the governing pressure (intermolecular water pressure) for defining water phase change; and (2) unable to account for variations in latent heat of fusion and water density. A new paradigm based on soil sorptive potential (SSP) to predict the SFC from the soil water retention curve is developed, directly using the intermolecular water pressure distribution and pure water phase diagram in lieu of capillary pressure and the Clapeyron equation. The latest theory of SSP is used to quantify intermolecular water pressure distribution. Experimental validation demonstrates that the proposed paradigm yields excellent matches to the experimental SFC data for different soil types, and is a significant improvement over the predictions by the capillary pressure-based Clapeyron equation paradigm. The proposed paradigm reveals that the SFCs for various soils below 273.15 K (0°C) are mostly dominated by adsorptive water. Furthermore, the proposed paradigm can fully explain the practically encountered phenomenon that the SFC for soils with high clay content depends on the initial water content, whereas it does not for sandy soils. Practical significance of the new paradigm in geotechnical engineering problems is demonstrated through predicting soil moisture profiles under freezing and thawing, and permafrost environments. **DOI: 10.1061/(ASCE)GT.1943-5606.0002597.** © 2021 American Society of Civil Engineers.

**Author keywords:** Soil freezing curve (SFC); Permafrost; Soil water retention curve; Soil sorptive potential (SSP); Pore water pressure; Matric suction.

#### Introduction

In nature, soil water remains partially unfrozen below 273.15 K (0°C) and above 251.17 K (-21.98°C), due to the soil-water physicochemical interaction including four well-known components: van der Waals, electrical double layer, osmotic, and hydrations (Lu and Zhang 2019; Zhang and Lu 2020). Below 251.17 K (-21.98°C), soil water will unfailingly exhibit either a solid or glassy state, dictated by the phase diagram of water (Dunaeva et al. 2010). Because different soils have different mineralogy, particle, and pore size distributions, their interaction with water leads to different freezing points. As such, the relationship between unfrozen water content and temperature is a constitutive function called the soil freezing curve (SFC). The SFC plays a governing role in many of soil's engineering properties such as the variation of hydraulic conductivity, elastic modulus, thermal conductivity, and shear strength in subzero temperature (e.g., Benson and Othman 1993; Painter and Karra 2014), and thereby is a fundamental constitutive relation underpinning many geotechnical engineering problems in cold regions, and

Note. This manuscript was submitted on August 18, 2020; approved on April 23, 2021; published online on June 28, 2021. Discussion period open until November 28, 2021; separate discussions must be submitted for individual papers. This paper is part of the *Journal of Geotechnical and Geoenvironmental Engineering*, © ASCE, ISSN 1090-0241.

risk assessment of geotechnical infrastructures in facing of global climate change. For example, SFC has been implemented to assess transportation geotechnical infrastructure durability subject to freeze—thaw cycles (e.g., de Grandpré et al. 2012; Ren and Vanapalli 2018), and slope failure induced by temperature fluctuations (e.g., Korshunov et al. 2016).

Extensive research efforts have been made to establish physical models for SFC (e.g., Koopmans and Miller 1966; Miller 1980; Kurylyk and Watanabe 2013; Zhang et al. 2018). Yet the existing approaches to establishing SFC are either empirical (e.g., Taylor and Luthin 1978) or mainly built on the Clapeyron equation (Koopmans and Miller 1966; Miller 1980; Liu and Yu 2013; Zhou et al. 2018) (see Appendix I). The existing paradigms in developing SFC are subject to several limitations: (1) incomplete definition of pore water pressure, (2) uncertainty in subjectively classifying soils into either adsorption or capillarity dominated types, and (3) inability in capturing varying latent heat and water density. These limitations will be elaborated in the next section. As a result, two practical challenges prevent the rigorous use of existing paradigms in predicting SFC: unable to use the governing pressure (intermolecular water pressure) for defining water phase change and unable to account for variations in latent heat of fusion and water density. Resolving the two practical challenges underpins a general SFC model for engineering practice yet is hindered by the use of the classical definition of matric potential as pore water pressure. Herein, to overcome the two inherent challenges in the common paradigms for SFC, a new paradigm is proposed based on the intermolecular pressures (i.e., the local water pressure at the intermolecular scale) of pore water or pore ice. The existing paradigm for SFC will be critically assessed to identify its limitations. A physical link based on soil sorptive

<sup>&</sup>lt;sup>1</sup>Professor, Ministry of Education Key Laboratory of Building Safety and Energy Efficiency, College of Civil Engineering, Hunan Univ., Changsha 410082, China (corresponding author). ORCID: https://orcid.org/0000-0002-6675-3940. Email: chao\_zhang@hnu.edu.cn

<sup>&</sup>lt;sup>2</sup>Professor, Dept. of Civil and Environmental Engineering, Colorado School of Mines, 1012 14th St., Golden, CO 80401. Email: ninglu@mines.edu

potential (SSP) is established between intermolecular water pressure and matric potential, leading to a new conceptual SFC model. Thereafter, the SSP-based paradigm is developed and quantitatively assessed with experimental data.

## Limitations in the Existing Paradigms

The theoretical basis underpinning almost all the physically-based SFC models is the analogy of soil freezing processes to soil drying processes. As such, the soil water retention curve (SWRC) models could be handily used to develop SFC models. In general, a physically-based SFC model is in terms of three physical links: (1) establishing the physical link between matric potential and the pore ice/water pressure at the freezing front; (2) estimating matric potential as a function of water content via SWRC models; and (3) determining the freezing temperature of the pore water at the freezing front via a certain form of the Clapeyron equation. Substituting the first two physical links into the third one yields an SFC model.

Pioneered by Koopmans and Miller (1966), the first physical link is commonly expressed as (e.g., Koopmans and Miller 1966; Miller 1980; Kurylyk and Watanabe 2013; Liu and Yu 2013)

$$p_{\rm i} - p_{\rm ufw} = \frac{1}{\lambda} (p_{\rm a} - p_{\rm w}) = -\frac{1}{\lambda} \psi_{\rm m} \tag{1}$$

where  $p_i$  and  $p_{ufw}$  are the ice pressure and unfrozen water pressure, respectively, in frozen soils;  $p_a$  and  $p_w$  are the air pressure and water pressure, respectively, in unsaturated soils;  $\lambda$  is a coefficient depending on soil types, equal to 1.0 for SLS (solid-liquid-solid) soils and equal to 2.2 for solid-solid (SS) soils (Koopmans and Miller 1966); and  $\psi_{\rm m}$  is matric potential, and is defined as the free energy (transferrable energy) difference per unit volume of water between the soil water state and free water state (Lu and Zhang 2019). The definition of matric potential is on the soil-water-air representative elementary volume (REV) shown in Fig. 1. The SLS soils and SS soils are conceptualized by Koopmans and Miller (1966) to facilitate the development of Eq. (1). A soil will be classified as an SLS soil when its soil-water interaction is only adsorption. In contrast, an SS soil interacts with water only via capillarity. The second physical link is usually represented by some classical SWRC models [e.g., van Genuchten (VG) model (van Genuchten 1980)], or some advanced SWRC models [e.g., Durner's model (Durner 1994)]. The third physical link is frequently represented by different forms of the Clapeyron equation.

Albeit widely adopted, these three physical links are subject to uncertainties or physically unjustified assumptions. In the first

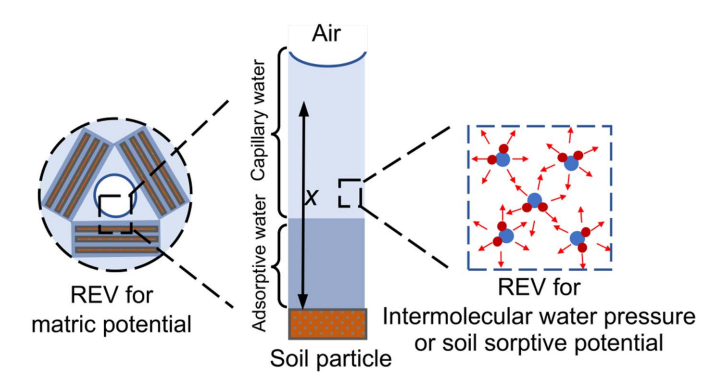


**Fig. 1.** Conceptual illustration of REVs for matric potential, intermolecular water pressure, and SSP.

physical link [Eq. (1)], one tacit assumption is that matric potential equals to capillary pressure  $(p_w-p_a)$ . This assumption indicates that under given matric potential the pore water pressure within the soil water-air REV will be uniform and negative (i.e., lower than ambient air pressure), suggesting that pore water is under tension and thereby exhibits a lower density than free water. However, the soil water density has been observed to be higher than free water (e.g., Zhang and Lu 2018a), and physical evidence indicates that the water pressure varies greatly at locations close to the solidwater interface (e.g., Mitchell 1960). If neglecting soil water density variation, it could be overestimated of matric potential by as much as 68%, of volumetric water content by up to 40%, and of specific surface area (SSA) by 42% (Zhang and Lu 2018b), thereby posing difficulties in characterizing engineering behavior of swelling soils (e.g., Villar and Lloret 2004; Richards and Bouazza 2007; Jacinto et al. 2012). In addition, the value of coefficient  $\lambda$  is subject to a great uncertainty because the fact that classifying a soil to be either a capillary or adsorptive type is subjective and not physically justified.

It has been long recognized that both adsorption and capillarity contribute to soil water retention (SWR) (e.g., McQueen and Miller 1974; Lu and Likos 2004). The adsorptive water is prominent for soils with high SSA [e.g., up to 0.243 g/g for Wyoming montmorillonite (Lu 2016)]. Nevertheless, to date, only a handful of models are able to explicitly account for both adsorption and capillarity (Revil and Lu 2013; Lu 2016). Yet none of these models has been used in developing SFC models due to their inability in capturing water pressure induced by adsorption. Among the existing SFC models, the second physical link is represented by the SWRC models that are based on capillary pressure.

In the third physical link, the latent heat and water density are two necessary input parameters for the Clapeyron equation. In spite of the research effort by Spaans and Baker (1996) in considering latent heat variation, both the latent heat of fusion and water density have also been usually treated as constants in the existing models, while in fact they can vary significantly with temperature; the latent heat can vary up to around 2 times (e.g., Bertolini et al. 1985; Spaans and Baker 1996; Cantrell et al. 2011), and the soil water density can increase up to 1.8 times (e.g., Zhang and Lu 2018b). Consequently, the Clapeyron equation deviates significantly from the phase transition boundary in the pure water phase diagram, yielding up to 86% smaller pressure under certain temperature, as illustrated in Fig. 2 (see Appendix I for a description of the Clapeyron equation).

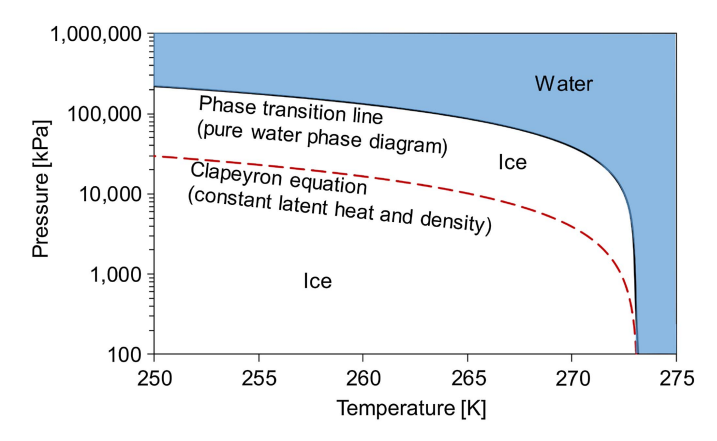


**Fig. 2.** Illustration of errors in direct use of the Clapeyron equation with constant latent heat and water density through comparisons of the Clapeyron equation (see Appendix I) and the phase transition line in the pure water phase diagram. (Data from Dunaeva et al. 2010.)

The aforementioned uncertainties and assumptions lead to several unresolved problems of both theoretical and practical importance. It is unclear on how to develop a physically sound SFC for unsaturated soils (e.g., Spaans and Baker 1996; Kurylyk and Watanabe 2013). The existing SFC models (Koopmans and Miller 1966; Miller 1980; Kurylyk and Watanabe 2013) commonly treated the soil water as either adsorptive water or capillary water despite the fact that the adsorptive water always coexists with the capillary water (e.g., Or and Tuller 1999; Lu 2016; Zhang and Liu 2018). To date, no SFC model is available to unify both adsorptive and capillary water retention mechanisms. Furthermore, it is unresolved how and whether the SFC depends on initial water content (Iwata et al. 1995; Kurylyk and Watanabe 2013). In nature, most of land surface is covered by unsaturated soils rather than saturated soils. Therefore, it is of practical importance to assess and quantify the role of initial water content in SFC.

These limitations will be circumvented in the proposed paradigm. Specifically, the physical link between matric potential and intermolecular water/ice pressure will be established by the SSP theory (Lu and Zhang 2019; Zhang and Lu 2020), which is able to delineate the adsorptive and capillary water pressure in soil. The physical link between matric potential and water content will be represented by a generalized SWRC model, which can explicitly separate a soil's adsorptive water and capillary water. The physical link between intermolecular water/ice pressure and freezing temperature will be represented by the phase diagram of pure water, avoiding the uncertainty in accounting variation in the latent heat and water density.

# Linking Intermolecular Water Pressure to Matric Potential

Fundamentally, the phase transition behavior of water is fully governed by the thermodynamic state variables of pressure and temperature defined at the REV of the intermolecular scale, which could be much smaller than the soil–water–air REV for matric potential that is controlled by the largest particle size, as shown in Fig. 1. Physically, it determines the phase condition of water or the freezing temperature of soil water. Recently, SSP was proposed and verified (Lu and Zhang 2019; Zhang and Lu 2020) to quantify the intermolecular water pressure variation in soils.

SSP is defined as the free energy change in a unit volume of soil water induced by the interaction of water molecules with external components of the system such as particle surface hydroxyls, exchangeable cations, and the solid substrate (Lu and Zhang 2019; Zhang and Lu 2020). The SSP consists of four well-known components: van der Waals, electrical, osmotic, and hydration. For sandy soils, the van der Waals component is the dominant one and retains thin film water coating soil particles. For silty and clayey soils, the SSP synthesizes the electromagnetic potentials of van der Waals, electrical double layer, and cation and surface hydration in the soil—water system. The SSP ( $\psi_{\text{sorp}}$ ) is recognized as the physical source for both matric potential and intermolecular water pressure and thereby provides a rigorous physical link between matric potential [ $\psi_{\text{m}}(w)$ ] and intermolecular water pressure ( $p_{\text{w}}$ ) (Lu and Zhang 2019; Zhang and Lu 2019)

$$p_{w}(x, w) = \psi_{m}(w) - \psi_{sorp}(x) + p_{a}$$
 (2)

where  $p_a$  is the ambient air pressure (kPa); w is the gravimetric water content (g water/g dry soil); x is the statistical average distance to the adjacent particle surface (Lu and Zhang 2019); and  $\psi_{\rm m}(w)$  is a function of water content (w) (i.e., the SWRC or water isotherm) (see Appendix II for a description for equations for

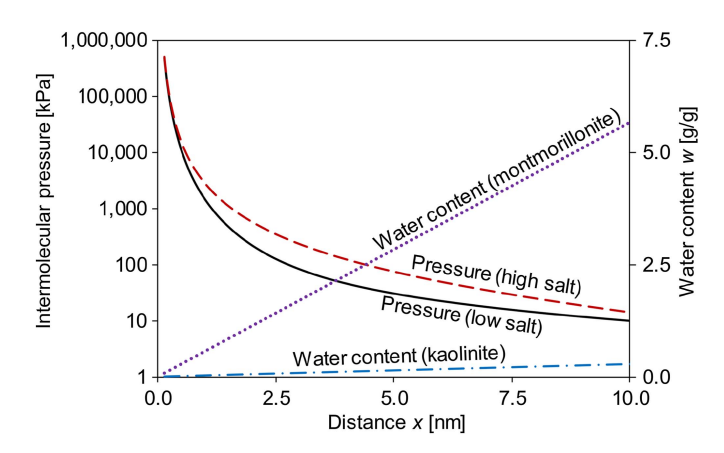


**Fig. 3.** Semi-quantitative illustration of intermolecular water pressure and upscaled water content as a function of distance *x* from the particle surface with different chemical concentrations in the pore water. (See Appendix III for material parameters.)

SWRC). The SWRC can be expressed explicitly by both adsorptive and capillary SWR mechanisms (Lu 2016).

The intermolecular water pressure induced by the SSP can vary dramatically with the distance (x) and can be as high as 506 MPa near the particle surface, as illustrated in Fig. 3. As such, the intermolecular water pressure is highly compressive near the particle surface rather than being negative (below air pressure). The statistical distance x can be scaled to gravimetric water content (w) (upscaled water content in Fig. 3) with the specific surface area (SSA) and averaged soil water density  $\rho_{\rm w}^{\rm ave}(w)$  by using a scaling equation:  $x = w \rho_{\rm w}^{\rm ave}(w)/{\rm SSA}$ . For example, for montmorillonite, a distance of 2 nm corresponds to w = 1.14 g/g. This suggests that, in montmorillonite with SSA = 567 m<sup>2</sup>/g, for water content <1.14 g/g or in  $x \le 2$  nm, the pore water pressure can be higher than 572 kPa (Fig. 3). Thus, it can be inferred that the intermolecular water pressure is remarkably high in clayey soils with large SSA.

## **Conceptual Soil Freezing Curve Model**

The freezing process is frequently considered analogous to the drying process because both displace soil water with another substance, that is, ice during freezing and air during drying (e.g., Koopmans and Miller 1966; Miller 1980; Zhang and Liu 2018). This analogy has been the physical basis for developing many SFC models from the SWRC. Here, the authors use this analogy to conceptualize the SFC.

Adsorption stems from the direct attraction between water and soil, and capillarity involves the interaction among soil, air, and water. These two SWR mechanisms are underpinned by the intermolecular forces of distinct energetic levels (Zhang and Lu 2018b): the former by the SSP with lower or more negative energy levels, and the latter by the surface tension of water with a relatively higher or less negative energy level. The energy levels of these intermolecular forces prescribe a unique SWR sequence with a sharp transition from adsorption to capillarity with increasing water content. Accordingly, the SWRC can be physically divided into three regimes: I–tightly adsorptive, II–adsorptive film, and III–capillary (Lu 2016) [as shown in Figs. 4(a and b)]. Regimes I and III are solely contributed respectively by adsorption and capillarity, whereas Regime II is the transition zone.

Conventionally, the Clapeyron equation is used to link freezing temperature in the SFC to matric potential in the SWRC model, but the existing SFC models deviate on which mathematical form of

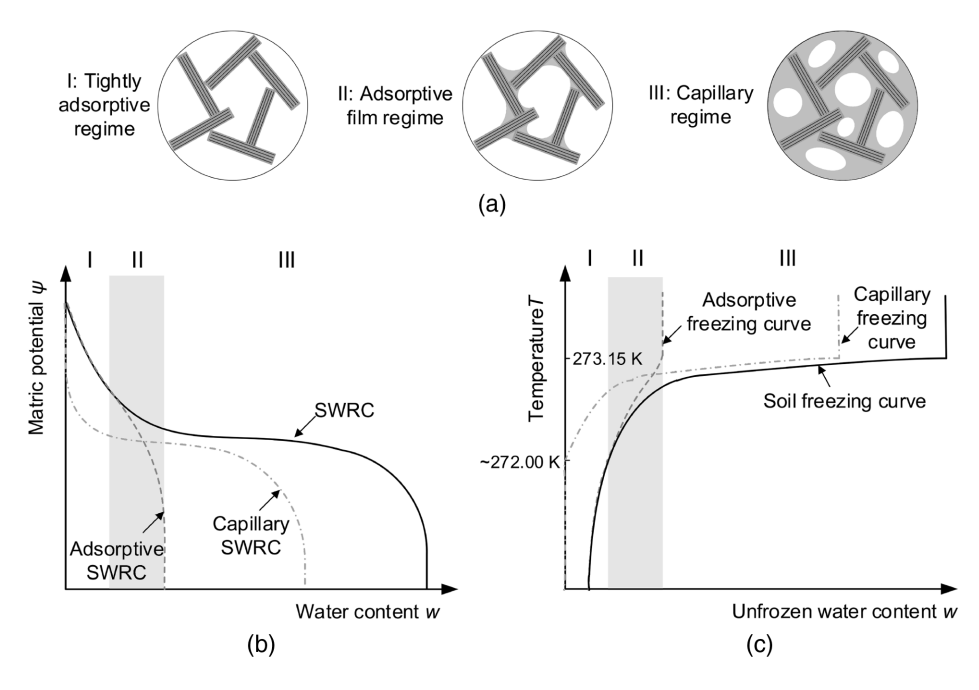


Fig. 4. Conceptual illustration of (a) soil water retention regimes; (b) generalized SWRC (adapted from Lu 2016); and (c) general paradigm for SFC.

the Clapeyron equation should be adopted. In these SFC models, the freezing temperature is unfailingly expressed as an increasing function of matric potential, suggesting a unique relation between temperature and matric potential. Then, it can be inferred from the SWR sequence that the SFC also exhibits a sharp transition from capillarity to adsorption with decreasing temperature (Zhang et al. 2018; Zhang and Liu 2018).

A general paradigm for SFCs can be conceptualized as a combination of two distinct branches with adsorptive and capillary freezing limbs as illustrated in Fig. 4(c). Upon decreasing temperature, the capillary water will freeze first because it exhibits relatively high chemical potential. Therefore, in the high-temperature range (> ~272.0 K or  $-1.15^{\circ}$ C), the SFC is mainly controlled by the freezing of capillary water, shown in Fig. 4(c). At a certain temperature (~272.0 K or  $-1.15^{\circ}$ C), the freezing of capillary water is almost complete, and the adsorptive water with its relatively high pressure induced by the SSP begins to freeze. Consequently, in the low-temperature range (< ~272.0 K or  $-1.15^{\circ}$ C), the SFC is dominated by the adsorptive freezing curve, shown in Fig. 4(c).

# A General Paradigm for Soil Freezing Curves

A new paradigm to predict the SFC from the SWRC is proposed and developed herein in two steps. First, the intermolecular water/ice pressure is determined as a function of water content with the aid of SSP and SWRC or water isotherm. Then, the freezing temperature is calculated as a function of the intermolecular water/ice pressure using a pure water phase transition line equation.

#### Intermolecular Water/Ice Pressure in Frozen Soils

The writers use the pressure equilibrium across the water–ice interfaces to define the intermolecular water/ice pressure in frozen soils. There are mainly two types of water–ice interfaces in frozen soils, shown in Figs. 5(a and b). In the zones far from the particle surface, the water–ice interface is beyond the influence zone of SSP. Such water–ice interface is governed by capillarity and is stretched by the water–ice interfacial tension to be concave into the liquid water phase (Liu et al. 2003; Zhang et al. 2018), as shown in Fig. 5(a).

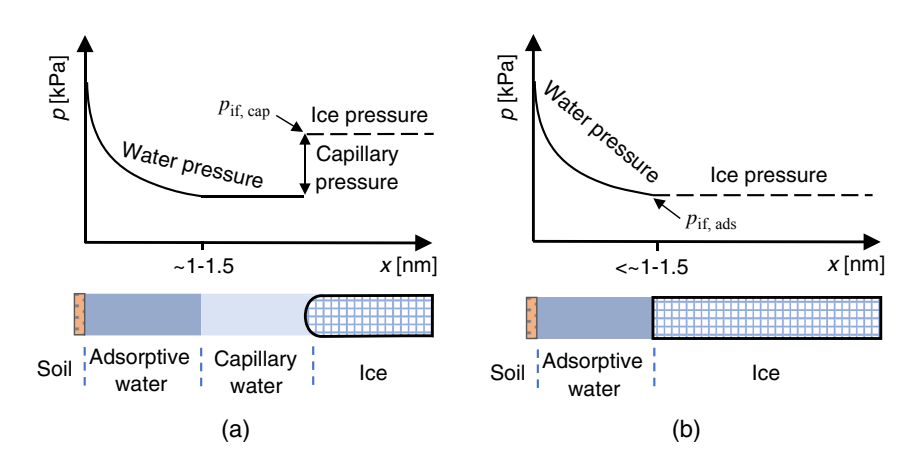


Fig. 5. Conceptual pressure profiles across the ice-water interface for (a) capillary regime; and (b) tightly adsorptive regime.

In the zones close to the particle surface, the water–ice interface is governed by adsorptive forces. To maintain chemical potential equilibrium, the water–ice interface develops with the same magnitude of adsorptive forces, that is, SSP. Considering the SSP is an increasing function of the statistical distance (Lu and Zhang 2019), the water–ice interface exhibits the same statistical distance to the particle surface (i.e., flat interface) as illustrated in Fig. 5(b).

The concave water—ice interface produces a pressure discontinuity across the interface, suggesting an increase in the ice pressure at the freezing front (Zhang et al. 2018), shown in Fig. 5(a). Under the increased pressure, the thermodynamic stability of ice decreases, depressing the freezing/melting temperature of water/ice. Considering the analogy between interfaces of water—ice and water—air, the ice pressure at the freezing front for capillary water ( $p_{\rm if,cap}$ ) can be written as a function of matric potential

$$p_{\text{if,cap}}(x, w) = -\psi_{\text{m}}(w) + p_{\text{a}}$$
(3)

In the tightly adsorptive regime, the water–ice interface is flat and indicates no pressure discontinuity across the interface. Consequently, the adsorptive ice pressure at the freezing front is equal to the adjacent intermolecular water pressure, as illustrated in Fig. 5(b). The adsorptive ice pressure highly depends on the location of the water–air interface at the initial water content ( $w_{\text{initial}}$ ) [i.e., the total water content before freezing (> 273.15 K)].

If the initial water content  $w_{\rm initial}$  is higher than maximum adsorptive water content  $w_{\rm amax}$ , the water–air interface is beyond the statistical distance x corresponding to  $w_{\rm amax}$  (i.e., the location of outermost adsorptive water). In this case, the intermolecular pressure of the outermost adsorptive water can be determined as identical to the adjacent capillary ice pressure. The intermolecular water pressure inside the outermost adsorptive water can be determined via Eq. (1). Therefore, in this case, the ice pressure at the freezing front for adsorptive water ( $p_{\rm if,ads}$ ) can be calculated as

$$p_{\rm if,ads}[w(x)] = p_{\rm if,cap}(w_{\rm amax}) - \psi_{\rm sorp}[w(x)] \quad \text{if } w_{\rm initial} \ge w_{\rm amax}$$
(4)

If  $w_{\text{initial}}$  is lower than  $w_{\text{amax}}$ , the water-air interface is within the statistical distance x corresponding to  $w_{\text{amax}}$ . In this case, the outermost adsorptive water is marked as the water-air interface. As such, the intermolecular pressure of the outermost adsorptive water is equal to the ambient air pressure, as demonstrated by Zhang and Lu (Zhang and Lu 2020). Considering Eq. (1), in this case, the ice pressure at the freezing front for adsorptive water can be written

$$p_{\rm if,ads}[w(x)] = \psi_{\rm m}(w_{\rm initial}) + p_{\rm a} - \psi_{\rm sorp}[w(x)] \quad {\rm if} \ w_{\rm initial} < w_{\rm amax} \eqno(5)$$

Summarizing Eqs. (4) and (5), the ice pressure at the freezing front for adsorptive water can be determined as

$$p_{\rm if,ads}[w(x)] = \begin{cases} p_{\rm if,cap}(w_{\rm amax}) - \psi_{\rm sorp}[w(x)] & \text{if } w_{\rm initial} \ge w_{\rm amax} \\ \psi_{\rm m}(w_{\rm initial}) + p_{\rm a} - \psi_{\rm sorp}[w(x)] & \text{if } w_{\rm initial} < w_{\rm amax} \end{cases}$$

$$(6)$$

#### Determination of Freezing or Fusion Point

The phase transition temperature is well defined as a function of pressure by the phase transition lines in the pure water phase diagram (e.g., Dunaeva et al. 2010). As to the phase transition line between ice and liquid water, the freezing/melting temperature can be calculated from the pressure as (Dunaeva et al. 2010)

$$\begin{split} \mathbf{T}_{\rm f}(p_{\rm if}) &= a + \mathbf{b}(0.0001 \times p_{\rm if}) + c \ln(0.0001 \times p_{\rm if}) \\ &+ e \sqrt{0.0001 \times p_{\rm if}} \end{split} \tag{7}$$

where  $T_{\rm f}$  is the freezing temperature in degrees kelvin;  $p_{\rm if}$  is the ice pressure in kPa, and it is equal to  $p_{\rm if,cap}$  for capillary water [Eq. (3)] and equal to  $p_{\rm if,ads}$  for adsorptive water [Eq. (6)]; and parameters a, b, c, and e are empirical coefficients: a=273.0159, b=-0.0132, c=-0.1577, and e=0.1516 (values from Dunaeva et al. 2010). These empirical coefficients were determined by fitting to the experimental data of phase transition of pure water. The valid situations are temperature from 251.165 to 273.15 K (-21.985 to 0°C); pressure from 0 to 208,566 kPa.

# **Experimental Validation**

#### Data Set for SWRCs and SFCs

To assess the variability of predicted general SFCs, a wide range of soils are selected and are categorized into four groups: kaolinite, bentonite, silty soil, and sandy soil (summarized in Table 1). Since it is difficult to find soil with both its SWRC and SFC, two soils under the same category are selected. Specifically, Wyoming montmorillonite (Likos and Lu 2003) and Umiat bentonite (Yoshikawa and Overduin 2005) are under the bentonite group because they have the same SSA of 800 m²/g (Anderson and Tice 1972), Georgia kaolinite (Likos and Lu 2003) and Georgia kaolinite (Anderson and Tice 1972) are under the kaolinite group, Arizona silty soil #4 (Jensen et al. 2015) and Fairbanks silt (Yoshikawa and Overduin 2005) are under the silty soil group, and Shonai dune sand (Mehta et al. 1994) and West Lebanon gravel <100  $\mu$ m (fractions with particle diameters smaller than 100  $\mu$ m) (Anderson and Tice 1972) are under the sandy soil group.

Table 1. Soil groups and names, origin, data content, and references for the soil data set

Soil group	Soil	Origin	Data content	Methods and references	
Kaolinite Georgia kaolinite		KGa-1b, Georgia, US	SWRC	VS, Likos and Lu (2003)	
	Georgia kaolinite		SFC	IC, Anderson and Tice (1972)	
Bentonite	Wyoming montmorillonite	Wyoming, US	SWRC	VS, Likos and Lu (2003)	
	Umiat bentonite	Alaska, US	SFC	FDR, TDT, and NMR, Yoshikawa and Overduin (2005)	
Silty soil	Arizona silty soil #4	Arizona, US	SWRC	VS, Jensen et al. (2015)	
	Fairbanks silt	Alaska, US	SFC	FDR, TDT, and NMR, Yoshikawa and Overduin (2005)	
Sandy soil	Shonai dune sand	Japan	SWRC	HWSM, PPA, and TP, Mehta et al. (1994)	
	West Lebanon gravel	New Hampshire, US	SFC	IC, Anderson and Tice (1972)	

Note: VS = vapor sorption; IC = isothermal calorimeter; FDR = frequency domain reflectometry; TDT = time domain transmissometry; NMR = nuclear magnetic resonance; HWSM = hanging water suction method; PPA = pressure plate apparatus; and TP = thermocouple psychrometer.

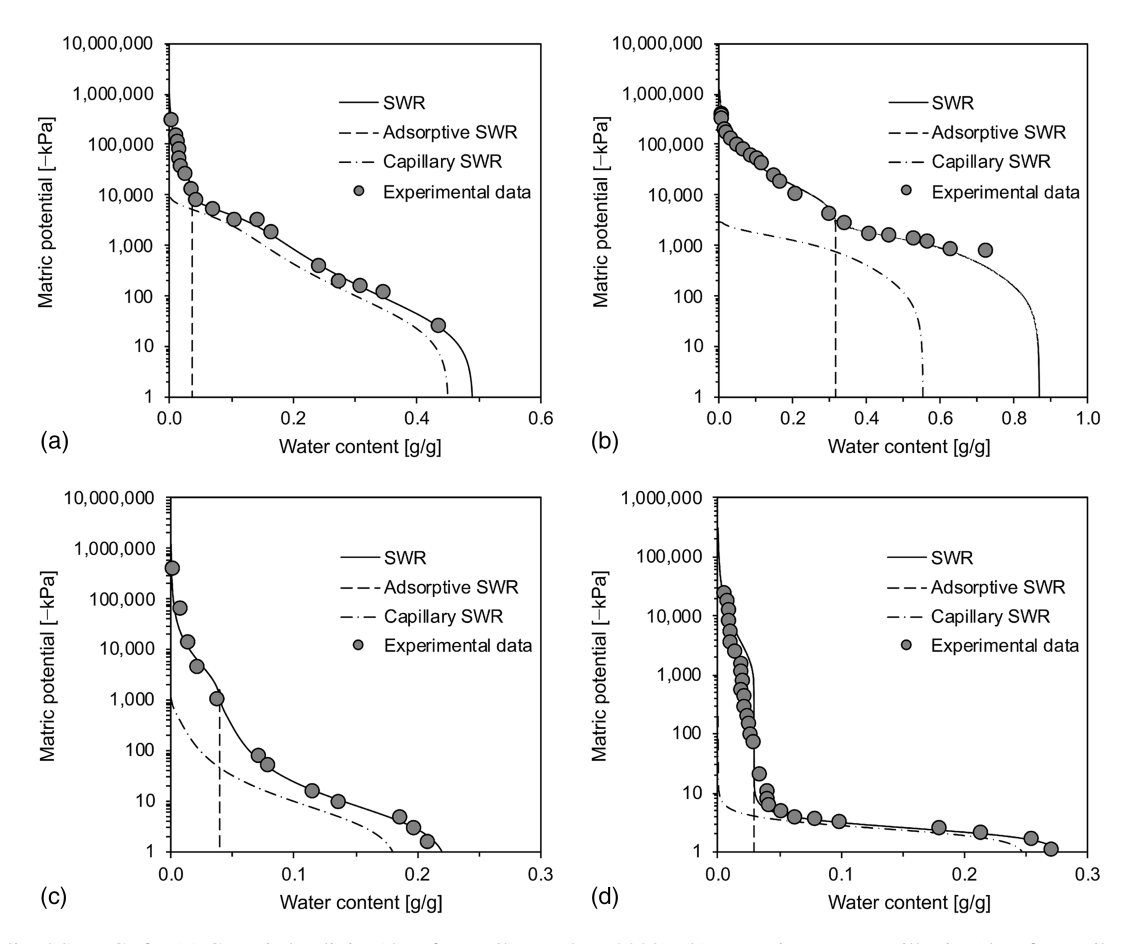


**Fig. 6.** Generalized SWRCs for (a) Georgia kaolinite (data from Likos and Lu 2003); (b) Wyoming montmorillonite (data from Likos and Lu 2003); (c) Arizona silty soil #4 (data from Jensen et al. 2015); and (d) Shonai dune sand (data from Mehta et al. 1994).

In general, excellent matches are achieved between experimental data and fitted Lu's SWRC model (see Appendix II for equations of Lu's SWRC model), and Lu's SWRC model explicitly separated the retained water content into capillary and adsorptive water contents, as illustrated in Figs. 6(a-d) (Lu 2016). The performance of Lu's SWRC model for a wide array of soils is elaborated in Lu (2016). The fitted curves are obtained via a least-square algorithm (Lu 2016). Based on the thermodynamic equilibrium at the water-air interface, it is recognized as the equivalence between the SSP and the adsorptive branch of the SWRC. As such, the SSP can be determined from SWRC model parameters as described in Zhang and Lu (2020). Fig. 7 illustrates the determined SSP curves for the selected soils with SWRC data content. The SSP is shown as a function of water content scaled from the statistical distance by using the scaled equation in Zhang and Lu (2020). In Fig. 7, the SSP generally nonlinearly decay with the increasing water content. The influence zone (water content range) of SSP significantly varies with the soil types. For examples, the influence zone of the SSP can be as high as w =0.32 g/g for Wyoming montmorillonite and as low as w = 0.03 g/gfor Shonai dune sand. The SSP of Shonai dune sand is weak because sandy soil has small specific surface area, and is only involved with the weakest SSP component: van der Waals attraction.

### Comparison

The SWRC model parameters are the only input parameters needed in the proposed SFC paradigm. As such, the SFC can be predicted by substituting the fitted SWRC parameters into Eqs. (3), (6), and (7). The fitted SWRC model parameters are summarized in

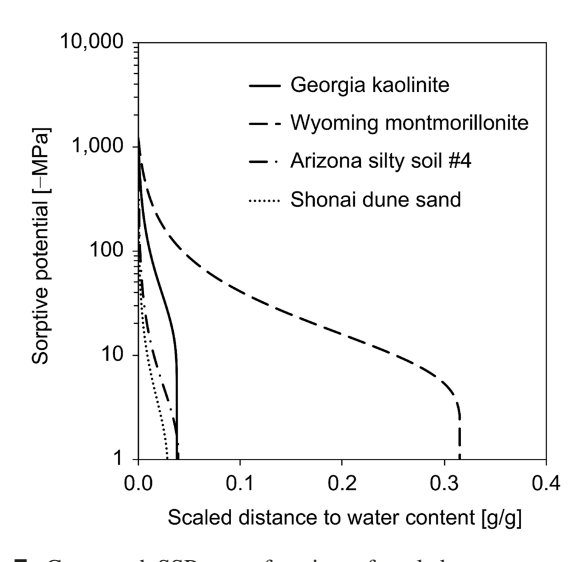
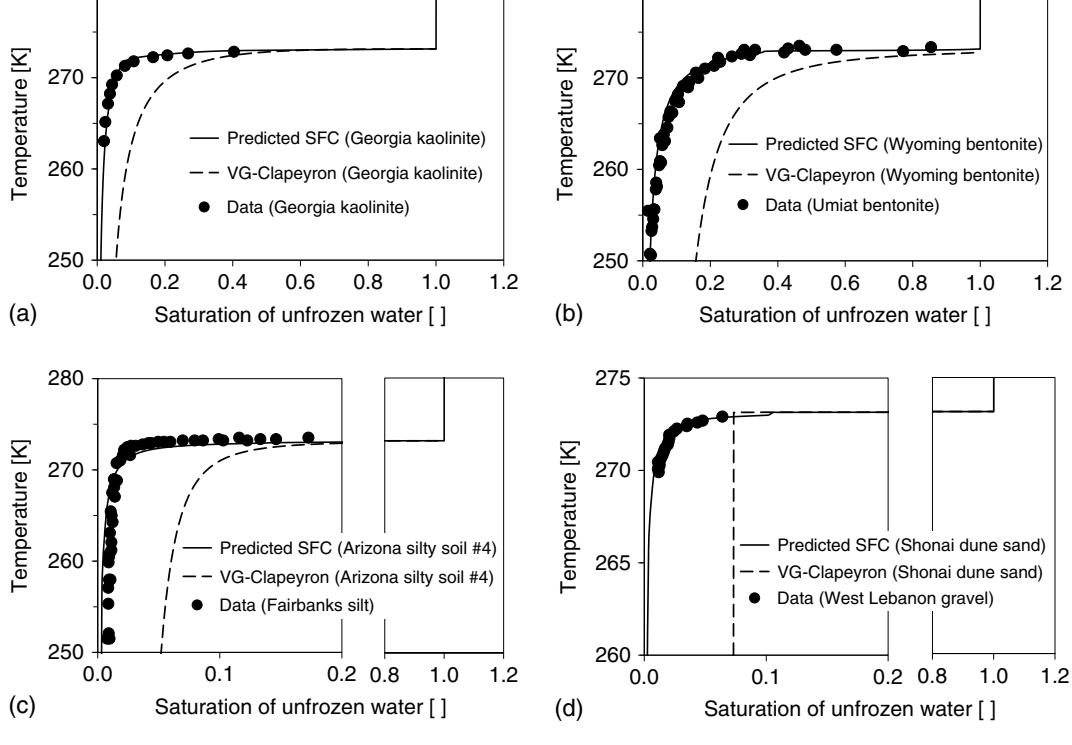


**Fig. 7.** Computed SSP as a function of scaled water content for selected soils.

Appendix II in SI units. The measured and predicted SFCs for the kaolinite soil group are compared in Fig. 8(a). The predicted SFC is based on the SWRC data from (Likos and Lu 2003). Although the SWRC and SFC are measured by different researchers, both Georgia kaolinite are KGa-1b Kaolin source clays from The Clay Minerals Society. As shown in Fig. 8(a), the predicted



280

**Fig. 8.** Comparisons among predicted SFC, the VG-Clapeyron model, and experimental data [from Anderson and Tice (1972) and Yoshikawa and Overduin (2005)] for soils with same mineral types: (a) bentonite group; and (b) kaolinite group, and for soils with same soil types: (c) silty soil group; and (d) sandy soil group.

SFC closely matches the experimental data, supporting the validity of the proposed SFC model and its determination paradigm.

280

The predicted and measured SFCs for the bentonite soil group are compared in Fig. 8(b). Researchers (Anderson and Tice 1972) observed that Umiat bentonite exhibit the same SSA and similar SFC with Wyoming montmorillonite. Therefore, it can be expected that the SFC of Wyoming montmorillonite should be similar to that of Umiat bentonite if the proposed SFC paradigm is valid. The predicted SFC for Wyoming montmorillonite closely matches with the measured SFC for Umiat bentonite, further supporting the validity of the proposed SFC model and its determination paradigm.

The measured SFCs of silty and sandy soil groups are selected to evaluate the applicability of the proposed SFC model to sandy and silty soils, as shown in Figs. 8(c and d). Since it is difficult to find soil with both its SWRC and SFC, two soils under the same category are selected. The SFCs are predicted with the SWRCs of the same soil types for comparisons. The predicted SFC of Arizona silty soil #4 closely matches the measured SFC of Fairbanks silt, as exhibited in Fig. 8(c). In addition, the predicted SFC of West Lebanon gravel <100  $\mu$ m shows good agreement with the predicted SFCs of the Shonai dune sand, as shown in Fig. 8(d). Therefore, it can be concluded that the proposed SFC is also applicable to silty and sandy soils. Further validation of the proposed SFC model requires the accurate measurement of both SWRC and SFC data for a wide array of soils.

The VG-Clapeyron model is a widely used method (e.g., Liu and Yu 2013) (see Appendix II for the VG-Clapeyron model). Considering the wide adoption of the VG model, the VG-Clapeyron model is selected to compare with the proposed SFC model. The VG SWRC parameters can be estimated by fitting the VG model with SWRC data, summarized in Appendix II. Substituting the fitted VG SWRC parameters into the VG-Clapeyron model yields the

predicted SFC, as shown in Figs. 8(a–d). It considers negative matric potential appeared in the VG SWRC model as the pressure in the Clapeyron equation to predict the SFC (e.g., Liu and Yu 2013) (see Appendix I). Generally, the VG-Clapeyron model tends to significantly overestimate the unfrozen water content. This overestimation is likely attributable to the adoption of the Clapeyron equation with constant latent heat and soil water density. In Fig. 8(d), the sharp decrease (vertical dashed lines) in the VG-Clapeyron model coincides the so-called residual water content in the VG SWRC model, and thereafter the unfrozen water content remains a constant equal to the residual water content. This illustrates that the VG-Clapeyron model is unable to incorporate the freezing of adsorptive water.

### Implications of SSP-Based Soil Freezing Curves

### Dependence of SFC on Soil Types

The SFCs for the four representative soils predicted by the proposed paradigm from their SWRCs are shown in Figs. 9(a–d). It shows that the proposed SFC model applies to a wide array of soils no matter whether the soil is dominated by adsorption or not. As temperatures decrease, the capillary water transforms first into ice, and the adsorptive water can persist in the liquid phase with decreasing temperatures. The temperature point at which the freezing of capillary water completes is: 272.9 K (–0.25°C) for Wyoming montmorillonite, 272.0 K (–1.15°C) for Georgia kaolinite, 272.9 K (–0.25°C) for Arizona silty soil #4, and 273.0 K (–0.15°C) for Shonai dune sand. The sandy soils generally do not exhibit small size pores due to their relatively large size particles. Therefore, the sandy soils cannot produce very negative capillary pressure, and the retained capillary water freezes at relatively high temperature compared to the capillary water in finer-grained soil.

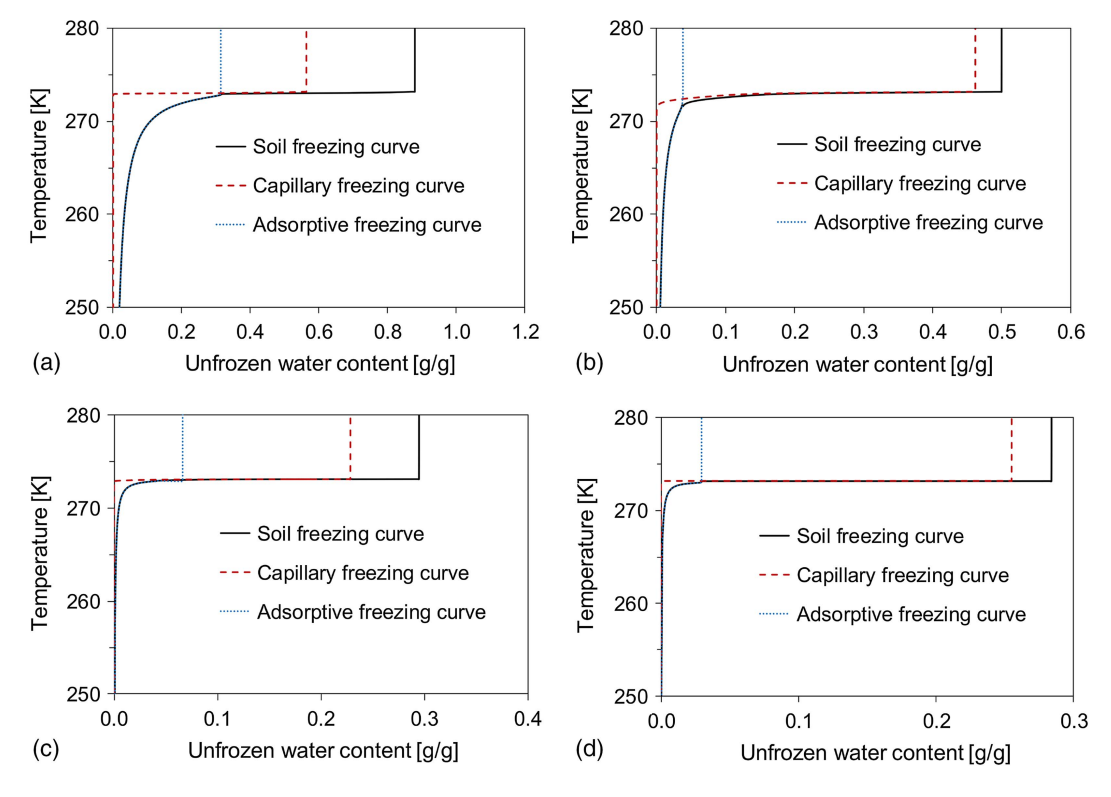


Fig. 9. Predicted SFCs for: (a) Wyoming montmorillonite; (b) Georgia kaolinite; (c) Arizona silty soil #4; and (d) Shonai dune sand.

The capillary water in Georgia kaolinite, in contrast, can persist in liquid phase down to 272.0 K ( $-1.15^{\circ}$ C) because its very fine particles yield small pores that can produce very low capillary pressures (Lu 2016). Below 273.12 K ( $-0.03^{\circ}$ C), the freezing of adsorptive water governs the SFCs of all the selected soils. Therefore, it can be concluded that the SFCs are mainly governed by the adsorptive water or the SSP, especially for temperature below 273.15 K ( $0^{\circ}$ C).

To further assess the variability of the predicted SFC paradigm, two parameters, maximum adsorptive water content ( $w_{\rm amax}$ ) and a pore-size distribution parameter (n, a parameter related to the capillary pore-size distribution) that controls the shape of SWRC in capillary regime, are selected for a sensitivity analysis. The maximum adsorptive water content essentially controls the adsorptive branch of SWRC. The unfrozen water content will significantly increase with increasing maximum adsorptive water

content, further highlighting the dominant role of adsorption in the SFC, as shown in Fig. 10(a). In contrast, the variation of pore-size distribution parameter n only imposes a marginal impact on the predicted SFC, rendering the subservient role of capillarity in the SFC.

#### Dependence of SFC on Initial Water Content

Experimental observations indicate that the unfrozen water content increases with increasing initial water content for soils with high clay content (Yong 1965; Tice 1978; Suzuki 2004; Wu et al. 2015). But this observed trend is not noticeable in sandy soil (Watanabe and Wake 2009). Despite abundant experimental observations, to date, no unified theory is available to explain this dependence of SFC on the initial water content. In the current theory, Eq. (5) states that the SFC depends on not only the SWRC model parameters but

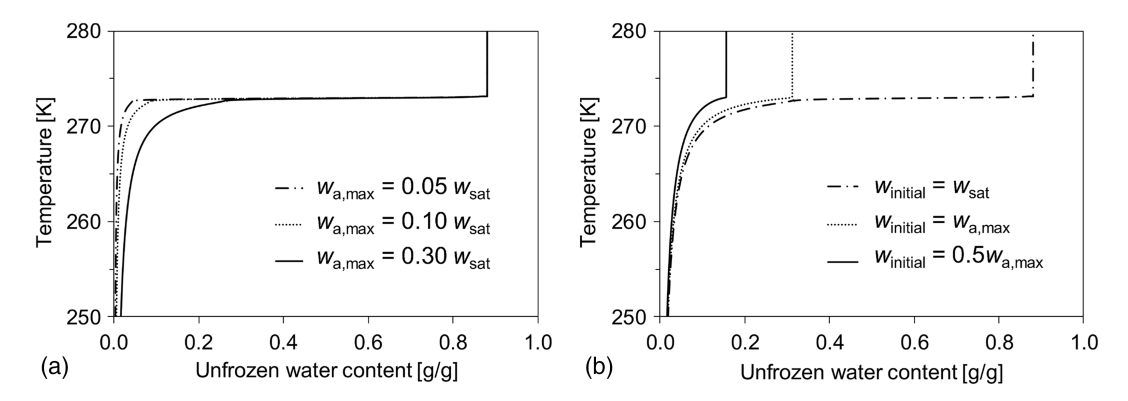


**Fig. 10.** (a) Effects of variation of maximum adsorptive water content ( $w_{\text{sat}}$ ) on predicted SFCs for Wyoming montmorillonite; and (b) dependence of predicted SFCs for Wyoming montmorillonite on initial water content ( $w_{\text{initial}}$ ).

also the initial water content. It is predicted that a decrease in initial water content will reduce the unfrozen water content, showing accordance with existing experimental observations (Yong 1965; Tice 1978; Suzuki 2004; Wu et al. 2015), as illustrated in Fig. 10(b). In addition, the proposed SFC paradigm attributes the dependence on the initial water content to the freezing of adsorptive water. It would be logically drawn from the current paradigm that soils with low clay content (low specific surface area) may not well demonstrate the dependence on the initial water content in the SFC, as observed by some researchers (Watanabe and Wake 2009). As such, the proposed SFC model qualitatively suggests that the controversy could be due to whether a soil exhibits sufficient SSA.

## Boundary between Capillarity and Adsorption

The predicted SFCs unfailingly show a temperature boundary marking the transition from capillary freezing curve to adsorptive freezing curve. This freezing temperature boundary varies from 272.0 K (-1.15°C) to 273.1 K (-0.05°C) for the selected soils, as shown in Figs. 9(a-d). In addition, the magnitude of capillary pressure is restricted by a threshold of cavitation pressure. Experimental data (Lu 2016) demonstrates that the cavitation pressure in soil is very unlikely to exceed -16 MPa (corresponding to 272.0 K (-1.15°C) in SFC). Hence, the unfrozen water content at 272.0 K (-1.15°C) can be treated as the lower bound of the maximum adsorptive water content for soils. Under this unique temperature point, the unfrozen water content will be fully dominated by adsorptive water. That is, the hydraulic conductivity of soil below -1.15°C will be governed by film flow of adsorptive water (e.g., Lebeau and Konrad 2010). This unique temperature point may provide a promising experimental way to determine the lower bound of the maximum adsorptive water content by measuring the unfrozen water content in soil at 272.0 K.

In addition, recent work (Lu 2016) shows that the maximum adsorptive water content for common soils does not exceed 30% of the saturated water content. Therefore, the measured SFCs can be evaluated by the criterion that the unfrozen water content at 272.0 K should be lower than 30% of the saturated water content. If the experimental data does not comply with this criterion, the algorithm underlying experimental techniques or experimental setup may not be valid.

# Practical Significance of the New Paradigm under Field Conditions

In cold regions, frozen soil's engineering behavior is inevitably involved in many geotechnical infrastructures. In recent years, global climate change poses new uncertainties or threats to the safety of natural slopes or engineered infrastructures, continuously challenging these infrastructure's resilience. Therefore, both traditional cold region geotechnical engineering and emerging geotechnical infrastructure's resilience urge a better understanding of soil's engineering properties under subzero temperature. The prerequisite underlying these engineering problems is to determine how much of water remains unfrozen under varying temperature (e.g., de Grandpré et al. 2012; Painter and Karra 2014; Korshunov et al. 2016; Ren and Vanapalli 2018). To fulfill this prerequisite, deliberate modeling of ground thawing and freezing processes under varying temperatures is required. The accuracy of such modeling process relies on the accuracy of the SFC models. Here, the writers selected two typical ground temperature profiles, as shown in Figs. 11(a-d), to illustrate how SFC models impact the unfrozen water content.

Two in situ temperature profiles were selected for the fields of seasonally frozen clayey soil (Lundin 1990) and permafrost silty soil (Hinkel et al. 2001), as shown in Figs. 11(a and b). The ground temperature varies with both depth and seasons, specifically dropping up to 25 K from summer to winter. To be representative, the SFC models of Wyoming montmorillonite and Arizona silty soil #4 were selected for the clayey soil and silty soil in the two fields, respectively. The saturation of unfrozen water profiles for the two fields were predicted by using the proposed SFC model and the VG-Clapeyron model for comparisons, as illustrated in Figs. 11(c and d). For the clay layer, the VG-Clapeyron model tends to vastly overestimate the unfrozen water content up to 3 times of that by the proposed SFC model, and therefore will likely yield much higher hydraulic conductivity, lower elastic modulus, and lower shear strength. For the silt layer, this overestimation is even higher, and up to 19 times. These comparisons show that SFC is a governing constitutive relationship for earthen infrastructures involving subzero temperature. It is expected that the proposed SFC paradigm will significantly improve the predictability, offering an opportunity to better predict soil's engineering behavior under freezing and thawing environments.

#### **Conclusions**

A new paradigm is developed for predicting SFCs by directly using intermolecular water pressure distribution and the pure water phase diagram, overcoming the inherent drawbacks of the commonly developed capillary pressure-based Clapeyron equation for modeling SFC. The intermolecular water pressure that governs soil—water phase transfer is highly dependent on SSP distribution around soil particles and can be quantified by experimental water isotherm data and a generalized SWR model. Experimental validation using the measured SFCs for a range of soil types demonstrates that the proposed paradigm can accurately predict the SFCs of all types of soils

By using the new paradigm, it is shown that unfrozen soil water below 273.15 K (0°C) is mostly dominated by adsorptive water, and the adsorptive water is under elevated pore pressure, leading to a clean physical explanation on why soil water resists freezing under low temperature. The proposed paradigm can fully explain the practically encountered, long-standing unresolved phenomenon that the SFC for soils with high clay content depends on the initial water content, whereas it does not for sandy soils. It is because that initial water content only impacts the freezing of adsorptive water but not for capillary water, and high clay content indicates a high adsorptive water content.

Practical significance of the new paradigm in geotechnical engineering problems is demonstrated through predicting soil moisture profiles under freezing and thawing, and permafrost environments. It is shown that the proposed paradigm can significantly improve the predictability of SFCs in earthen infrastructures under seasonally frozen and permafrost environments.

#### Appendix I. Clapeyron Equation

Most of the existing SFC models select different forms of the Clapeyron equation to determine the freezing temperature of water in soil (Konrad and Morgenstern 1980; Kurylyk and Watanabe 2013; Liu and Yu 2013; Watanabe and Flury 2008). One commonly used form of the Clapeyron equation can be written (e.g., Liu and Yu 2013; Zhang and Liu 2018)

$$T_{\rm f} = T_{\rm f0} \exp\left(\frac{p_i - p_{ufw}}{-\rho_w L_a}\right) \tag{8}$$

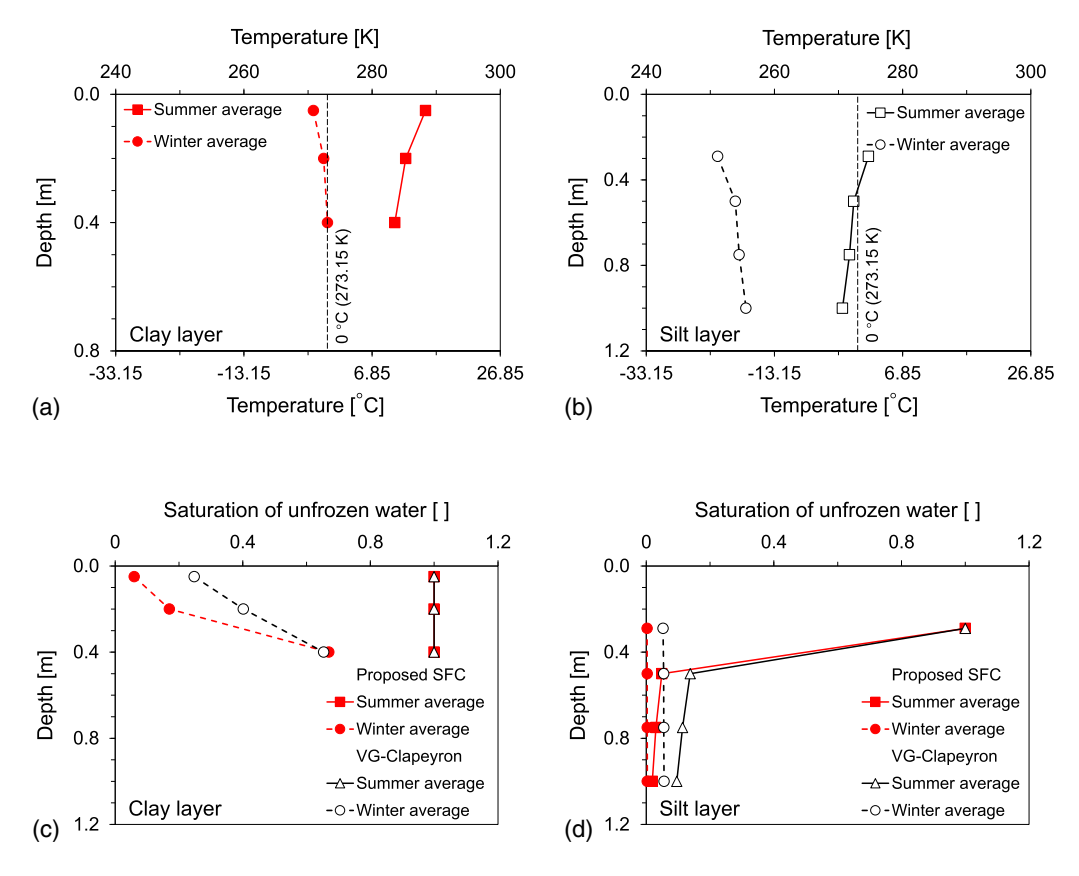


**Fig. 11.** Typical in situ temperature profiles of (a) seasonally frozen clay layer (data from Lundin 1990); and (b) permafrost silt layer (data from Hinkel et al. 2001). Comparisons of unfrozen water content profiles predicted by the proposed paradigm and VG-Clapeyron model in (c) clay layer; and (d) silt layer.

where  $T_{f0}$  is the freezing point of free water [i.e., 273.15 K (0 °C)];  $p_i$  and  $p_{ufw}$  are the ice pressure and unfrozen water pressure, respectively, in frozen soils;  $\rho_{\rm w}$  is the density of water; and  $L_a$  is the latent heat of water fusion.

The existing SFC models usually treat water density and latent heat as constant values. However, experimental evidence shows that both the water density and the latent heat are sensitive to pressure and temperature (e.g., Bertolini et al. 1985; Cantrell et al. 2011; Zhang and Lu 2018a, b), although no accurate mathematical functions have been established for these variations. The phase transition line equation [Eq. (7)] has been validated against numerous experimental data (Dunaeva et al. 2010), and thus can be used to evaluate the accuracy of the Clapeyron equation with constant water density and latent heat. It is shown in Fig. 2 that the Clapeyron equation with constant parameters significantly underestimates the freezing temperature, especially in the high-pressure range.

# Appendix II. SWRC Models

The LU SWRC model can be mathematically expressed as (Lu 2016)

$$w_{\rm t}(\psi_{\rm m}) = w_{\rm a}(\psi_{\rm m}) + w_{\rm c}(\psi_{\rm m}) \tag{9}$$

$$w_{\rm a}(\psi_{\rm m}) = w_{\rm a,max} \left\{ 1 - \left[ \exp\left(\frac{\psi_{\rm m} - \psi_{\rm min}}{\psi_{\rm m}}\right) \right]^m \right\} \tag{10}$$

$$w_{c}(\psi_{m}) = \frac{1}{2} \left[ 1 - \operatorname{erf}\left(\sqrt{2} \frac{\psi_{m} - \psi_{cav}}{\psi_{cav}}\right) \right] \times \left[ w_{sat} - w_{a}(\psi_{m}) \right] \left[ 1 + (\alpha \psi_{m})^{n} \right]^{1/n - 1}$$
(11)

where  $w_t$  is the total water content;  $w_a$  is the adsorptive water content;  $w_c$  is the capillary water content;  $w_{a,\text{max}}$  is the maximum adsorptive water content (g/g);  $\psi_{\text{min}}$  is the minimum or most negative matric potential (kPa or kJ/m³); m is the adsorptive strength;  $\psi_{\text{cav}}$  is the mean cavitation matric potential (kPa or kJ/m³);  $w_{\text{sat}}$  is the saturated water content (g/g); n is a parameter related to the capillary pore-size distribution; and  $1/\alpha$  is a parameter related to the air-entry matric potential (kPa).

The VG model for SWRC is expressed as (van Genuchten 1980)

$$\psi_{\rm m} = \frac{1}{\alpha} \left[ 1 - \left( \frac{w - w_{\rm r}}{w_{\rm sat} - w_{\rm r}} \right)^{-1/m} \right]^{1/n} \tag{12}$$

where  $w_r$  is the residual water content [g/g].

Assuming  $p_i - p_{\text{ufw}} = (1/\lambda)(p_a - p_w) = -(1/\lambda)\psi_m$  and  $\lambda = 1.0$  for clayey soils, the VG-Clapeyron model can be expressed as

$$T_{\rm f} = T_{\rm f0} \exp\left\{\frac{1}{-\rho_{\rm w} L_a} \frac{1}{\alpha} \left[1 - \left(\frac{w - w_{\rm r}}{w_{\rm sat} - w_{\rm r}}\right)^{-1/m}\right]^{1/n}\right\}$$
(13)

Table 2 summarizes the LU and VG SWRC model parameters of the selected soils with SWRC data content (i.e., Georgia kaolinite, Wyoming montmorillonite, Arizona silty soil #4, and Shonai dune sand). These parameters were obtained by fitting LU and

Table 2. Parameters for LU [Eqs. (9)-(11)] and VG [Eq. (12)] SWRC models of the SWRC data set

Soil	SWRC model	$\psi_{\min}$ (-kPa)	m	$\psi_{\rm cav}$ (-kPa)	$w_{\rm sat}~({\rm g/g})$	$w_{a,\text{max}}$ or $w_r$ (g/g)	n	$A (-kPa^{-1})$
Georgia kaolinite	LU	1,200,000	0.032	4,460	0.500	0.038	1.296	0.033
	VG	Infinity	7.975	N/A	0.500	0.007	0.386	0.000
Wyoming montmorillonite	LU	1,200,000	0.013	1,463	0.881	0.316	1.272	0.005
	VG	Infinity	0.043	N/A	0.881	0.000	11.485	0.002
Arizona silty soil #4	LU	1,200,000	0.004	555	0.230	0.040	1.654	0.223
	VG	Infinity	0.178	N/A	0.230	0.004	1.974	0.412
Shonai dune sand	LU	309,354	0.012	100	0.285	0.029	4.951	0.416
	VG	Infinity	0.461	N/A	0.285	0.020	5.565	0.492

Source: Data from Lu (2016).

VG SWRC models to experimental data. Both LU and VG SWRC models can well fit the experimental data ( $R^2 > 0.98$ ) (Lu 2016).

# Appendix III. Material Parameters

The curves in Fig. 3 are produced by following the theory proposed by Lu and Zhang (2019). The material parameters used in producing Fig. 3 are summarized here. Thickness of particle t=60 nm; Hamaker constant  $A_{\rm H}=2.5\times 10^{-20}$  J (Lu et al. 2008); Surface potential  $V_{\rm edl0}=250$  mV (Lu et al. 2008); ion concentration  $c_0=0.001$  mol/m³ for low salt, and  $c_0=1.0$  mol/m³ for high salt; hydration potential near the particle surface  $\psi_{\rm hyd0}=-3.2\times 10^5\,{\rm kJ/m}^3$  (Butt and Kappl 2009); decay length  $\lambda_{\rm h}=0.6$  nm (Butt and Kappl 2009); and SSA=567 m²/g for montmorillonite and SSA=28 m²/g for kaolinite (Khorshidi et al. 2017). Total potential is considered as  $\psi_{\rm t}=0.0$ . For other values of total potential, the corresponding intermolecular pressure profile can be calculated as a sum of the intermolecular pressure profile with  $\psi_{\rm t}=0.0$  and the value of total potential.

# **Data Availability Statement**

All data, models, and code generated or used during the study are available from the corresponding author upon reasonable request.

#### **Acknowledgments**

This research was sponsored by National Key R&D Program of China Grant (2019YFB1705201, 2019YFC1904704) and the US National Science Foundation Grants (NSF CMMI-1902045).

### References

- Anderson, D. M., and A. R. Tice. 1972. "Predicting unfrozen water contents in frozen soils from surface area measurements." *Highway Res. Rec.* 393 (2): 12–18.
- Benson, C. H., and M. A. Othman. 1993. "Hydraulic conductivity of compacted clay frozen and thawed in situ." *J. Geotech. Eng.* 119 (2): 276–294. https://doi.org/10.1061/(ASCE)0733-9410(1993)119:2(276).
- Bertolini, D., M. Cassettari, and G. Salvetti. 1985. "Anomalies in the 'latent heat' of solidification of supercooled water." *Chem. Phys. Lett.* 119 (6): 553–555. https://doi.org/10.1016/0009-2614(85)85387-2.
- Butt, H.-J., and M. Kappl. 2009. *Surface and interfacial forces*. Berlin: Wiley-VCH Verlag GmbH.
- Cantrell, W., A. Kostinski, A. Szedlak, and A. Johnson. 2011. "Heat of freezing for supercooled water: Measurements at atmospheric pressure." J. Phys. Chem. A 115 (23): 5729–5734. https://doi.org/10 .1021/jp103373u.

- de Grandpré, I., D. Fortier, and E. Stephani. 2012. "Degradation of permafrost beneath a road embankment enhanced by heat advected in groundwater." Can. J. Earth Sci. 49 (8): 953–962. https://doi.org/10.1139/e2012-018.
- Dunaeva, A. N., D. V. Antsyshkin, and O. L. Kuskov. 2010. "Phase diagram of H2O: Thermodynamic functions of the phase transitions of high-pressure ices." Sol. Syst. Res. 44 (3): 202–222. https://doi.org/10.1134/S0038094610030044.
- Durner, W. 1994. "Hydraulic conductivity estimation for soils with heterogeneous pore structure." Water Resour. Res. 30 (2): 211–223. https://doi.org/10.1029/93WR02676.
- Hinkel, K. M., F. Paetzold, F. E. Nelson, and J. G. Bockheim. 2001. "Patterns of soil temperature and moisture in the active layer and upper permafrost at Barrow, Alaska: 1993–1999." Glob. Planet. Change 29 (3–4): 293–309. https://doi.org/10.1016/S0921-8181(01)00096-0.
- Iwata, S., T. Tabuchi, and B. P. Warkentin. 1995. Soil-water interactions: Mechanisms and applications. Abingdon, UK: Taylor & Francis.
- Jacinto, A. C., M. V. Villar, and A. Ledesma. 2012. "Influence of water density on the water-retention curve of expansive clays." *Géotechnique* 62 (8): 657–667. https://doi.org/10.1680/geot.7.00127.
- Jensen, D. K., M. Tuller, L. W. de Jonge, E. Arthur, and P. Moldrup. 2015. "A new two-stage approach to predicting the soil water characteristic from saturation to oven-dryness." *J. Hydrol.* 521 (Feb): 498–507. https://doi.org/10.1016/j.jhydrol.2014.12.018.
- Khorshidi, M., N. Lu, I. D. Akin, and W. J. Likos. 2017. "Intrinsic relationship between specific surface area and soil water retention." *J. Geotech. Geoenviron. Eng.* 143 (1): 04016078. https://doi.org/10.1061/(ASCE) GT.1943-5606.0001572.
- Konrad, J.-M., and N. R. Morgenstern. 1980. "A mechanistic theory of ice lens formation in fine-grained soils." *Can. Geotech. J.* 17 (4): 473–486. https://doi.org/10.1139/t80-056.
- Koopmans, R. W. R., and R. D. Miller. 1966. "Soil freezing and soil water characteristic curves." *Soil Sci. Soc. Am. J.* 30 (6): 680. https://doi.org/10.2136/sssaj1966.03615995003000060011x.
- Korshunov, A. A., S. P. Doroshenko, and A. L. Nevzorov. 2016. "The impact of freezing-thawing process on slope stability of earth structure in cold climate." *Procedia Eng.* 143: 682–688. https://doi.org/10.1016/j.proeng.2016.06.100.
- Kurylyk, B. L., and K. Watanabe. 2013. "The mathematical representation of freezing and thawing processes in variably-saturated, non-deformable soils." *Adv. Water Resour.* 60 (Oct): 160–177. https://doi.org/10.1016/j.advwatres.2013.07.016.
- Lebeau, M., and J.-M. Konrad. 2010. "A new capillary and thin film flow model for predicting the hydraulic conductivity of unsaturated porous media." Water Resour. Res. 46 (Sep): 1–15. https://doi.org/10.1029 /2010WR009092.
- Likos, W., and N. Lu. 2003. "Automated humidity system for measuring total suction characteristics of clay." *Geotech. Test. J.* 26 (2): 10456. https://doi.org/10.1520/GTJ11321J.
- Liu, Z., K. Muldrew, R. G. Wan, and J. A. W. Elliott. 2003. "Measurement of freezing point depression of water in glass capillaries and the associated ice front shape." *Phys. Rev. E* 67 (6): 61602. https://doi.org/10 .1103/PhysRevE.67.061602.

- Liu, Z., and X. Yu. 2013. "Physically based equation for phase composition curve of frozen soils." *Transp. Res. Rec.* 2349 (1): 93–99. https://doi.org/10.3141/2349-11.
- Lu, N. 2016. "Generalized soil water retention equation for adsorption and capillarity." J. Geotech. Geoenviron. Eng. 142 (10): 04016051. https:// doi.org/10.1061/(ASCE)GT.1943-5606.0001524.
- Lu, N., M. T. Anderson, W. J. Likos, and G. W. Mustoe. 2008. "A discrete element model for kaolinite aggregate formation during sedimentation." *Int. J. Numer. Anal. Methods Geomech.* 32 (8): 965–980. https://doi.org/10.1002/nag.656.
- Lu, N., and W. J. Likos. 2004. *Unsaturated soil mechanics*. New York: Wiley.
- Lu, N., and C. Zhang. 2019. "Soil sorptive potential: Concept, theory, and verification." J. Geotech. Geoenviron. Eng. 145 (4): 04019006. https:// doi.org/10.1061/(ASCE)GT.1943-5606.0002025.
- Lundin, L. 1990. "Hydraulic properties in an operational model of frozen soil." *J. Hydrol.* 118 (1–4): 289–310. https://doi.org/10.1016/0022 -1694(90)90264-X.
- McQueen, I. S., and R. F. Miller. 1974. "Approximating soil moisture characteristics from limited data: Empirical evidence and tentative model." *Water Resour. Res.* 10 (3): 521–527. https://doi.org/10 .1029/WR010i003p00521.
- Mehta, B. K., S. H. O. Shiozawa, and M. Nakano. 1994. "Hydraulic properties of a sandy soil at low water contents." *Soil Sci.* 157 (4): 208–214. https://doi.org/10.1097/00010694-199404000-00002.
- Miller, R. D. 1980. "Freezing phenomena in soils." In Applications of soil physics, 254–299. Amsterdam, Netherlands: Elsevier.
- Mitchell, J. K. 1960. "Components of pore water pressure and their engineering significance." Clays Clay Miner. 9 (1): 162–184. https://doi.org/10.1346/CCMN.1960.0090109.
- Or, D., and M. Tuller. 1999. "Liquid retention and interfacial area in variably saturated porous media: Upscaling from single pore to sample-scale model." Water Resour. Res. 35 (12): 3591–3605. https://doi.org/10.1029/1999WR900262.
- Painter, S. L., and S. Karra. 2014. "Constitutive model for unfrozen water content in subfreezing unsaturated soils." *Vadose Zone J.* 13 (4): 1–8. https://doi.org/10.2136/vzj2013.04.0071.
- Ren, J., and S. K. Vanapalli. 2018. "Prediction of resilient modulus of frozen unbound road materials using soil-freezing characteristic curve." Can. Geotech. J. 55 (8): 1200–1207. https://doi.org/10.1139/cgj-2017-0153.
- Revil, A., and N. Lu. 2013. "Unified water isotherms for clayey porous materials." Water Resour. Res. 49 (9): 5685–5699. https://doi.org/10 .1002/wrcr.20426.
- Richards, S., and A. Bouazza. 2007. "Determination of particle density using water and gas pycnometry." *Géotechnique* 57 (4): 403–406. https://doi.org/10.1680/geot.2007.57.4.403.
- Spaans, E. J. A., and J. M. Baker. 1996. "The soil freezing characteristic: Its measurement and similarity to the soil moisture characteristic." Soil Sci. Soc. Am. J. 60 (1): 13. https://doi.org/10.2136/sssaj1996.0361599500 6000010005x.
- Suzuki, S. 2004. "Dependence of unfrozen water content in unsaturated frozen clay soil on initial soil moisture content." Soil Sci. Plant Nutr. 50 (4): 603–606. https://doi.org/10.1080/00380768.2004.10408518.

- Taylor, G. S., and J. N. Luthin. 1978. "A model for coupled heat and moisture transfer during soil freezing." *Can. Geotech. J.* 15 (4): 548–555. https://doi.org/10.1139/t78-058.
- Tice, A. R. 1978. "Determination of unfrozen water in frozen soil by pulsed nuclear magnetic resonance." In *Proc.*, 3rd Int. Conf. Permafrost, 149– 155. Edmonton, AB, Canada: National Research Council of Canada.
- van Genuchten, M. T. 1980. "A closed-form equation for predicting the hydraulic conductivity of unsaturated soils." *Soil Sci. Soc. Am. J.* 44 (5): 892. https://doi.org/10.2136/sssaj1980.03615995004400050002x.
- Villar, M. V., and A. Lloret. 2004. "Influence of temperature on the hydromechanical behaviour of a compacted bentonite." *Appl. Clay Sci.* 26 (1–4): 337–350. https://doi.org/10.1016/j.clay.2003.12.026.
- Watanabe, K., and M. Flury. 2008. "Capillary bundle model of hydraulic conductivity for frozen soil." Water Resour. Res. 44 (12): 1–9. https:// doi.org/10.1029/2008WR007012.
- Watanabe, K., and T. Wake. 2009. "Measurement of unfrozen water content and relative permittivity of frozen unsaturated soil using NMR and TDR." Cold Reg. Sci. Technol. 59 (1): 34–41. https://doi.org/10 .1016/j.coldregions.2009.05.011.
- Wu, M., X. Tan, J. Huang, J. Wu, and P.-E. Jansson. 2015. "Solute and water effects on soil freezing characteristics based on laboratory experiments." *Cold Reg. Sci. Technol.* 115 (Jul): 22–29. https://doi.org/10 .1016/j.coldregions.2015.03.007.
- Yong, R. N. 1965. "Soil suction effects on partial soil freezing." *Highway Res. Rec.* 68: 31–42.
- Yoshikawa, K., and P. P. Overduin. 2005. "Comparing unfrozen water content measurements of frozen soil using recently developed commercial sensors." *Cold Reg. Sci. Technol.* 42 (3): 250–256. https://doi.org/10.1016/j.coldregions.2005.03.001.
- Zhang, C., and Z. Liu. 2018. "Freezing of water confined in porous materials: Role of adsorption and unfreezable threshold." *Acta Geotech*. 13 (5): 1203–1213. https://doi.org/10.1007/s11440-018-0637-6.
- Zhang, C., Z. Liu, and P. Deng. 2018. "Using molecular dynamics to unravel phase composition behavior of nano-size pores in frozen soils: Does Young–Laplace equation apply in low temperature range?" Can. Geotech. J. 55 (8): 1144–1153. https://doi.org/10.1139/cgj-2016-0150.
- Zhang, C., and N. Lu. 2018a. "Measuring soil-water density by helium pycnometer." *J. Geotech. Geoenviron. Eng.* 144 (9): 02818002. https://doi.org/10.1061/(ASCE)GT.1943-5606.0001929.
- Zhang, C., and N. Lu. 2018b. "What is the range of soil water density? Critical reviews with a unified model." *Rev. Geophys.* 56 (3): 532–562. https://doi.org/10.1029/2018RG000597.
- Zhang, C., and N. Lu. 2019. "Unitary definition of matric suction." J. Geotech. Geoenviron. Eng. 145 (2): 02818004. https://doi.org/10.1061/(ASCE)GT.1943-5606.0002004.
- Zhang, C., and N. Lu. 2020. "Soil sorptive potential: Its determination and predicting soil water density." *J. Geotech. Geoenviron. Eng.* 146 (1): 04019118. https://doi.org/10.1061/(ASCE)GT.1943-5606.0002188.
- Zhou, J., C. Wei, Y. Lai, H. Wei, and H. Tian. 2018. "Application of the generalized Clapeyron equation to freezing point depression and unfrozen water content." Water Resour. Res. 54 (11): 9412–9431.